Available online at www.sciencedirect.com
SCIENCE DIRECT®
Journal of Photochemistry and Photobiology A: Chemistry 173 (2005) 21–28
Journal of Photochemistry and Photobiology A:Chemistry
www.elsevier.com/locate/jphotochem

Reversibility of conformational switching in light-sensitive peptides

Vitali Borisenko, G. Andrew Woolley*

Department of Chemistry, University of Toronto, 80 St. George St., Toronto, Canada M5S 3H6

Received 27 August 2004; received in revised form 20 December 2004; accepted 28 December 2004
Available online 26 January 2005

Abstract

Reversible photo-control of protein structure and function is used by Nature to direct complex biological response to light. Reversibility is a feature that has been difficult to reliably achieve in analogous biomimetic systems. We report here measurement of the thermal and photoisomerization rates for peptide model systems in which isomerization of an intramolecularly linked azobenzene unit causes a helix-coil transition in the peptide. Reversibility is maintained and indeed the quantum yield for *cis*-to-*trans* photoisomerization is enhanced in these systems compared to an unstructured glutathione adduct of the chromophore alone. Reversibility can be understood by considering the intrinsic conformational preferences of the peptides to which the linkers are attached and how these preferences impact the stabilities of the transition states for isomerization.

Keywords: Azobenzene; α-Helix-coil; Light-induced; Photo-control; Photo-isomerization

1. Introduction

Using light to control the activity of biomolecules is an attractive strategy for probing function in complex living systems. Photo-sensitive biomolecules can be introduced into cells and manipulated non-invasively with a high degree of spatial and temporal control [3,4]. For instance, caged compounds, in which a light flash is used to produce a step increase in the concentration of a bioactive species, have facilitated studies of muscle contraction, intracellular signalling, and neurotransmission [5,6]. Whereas, synthetic caged compounds undergo an essentially irreversible photochemical reaction, nature has evolved reversible means of coupling light signals to cellular chemistry as evidenced by the phototropic responses of plants via phytochromes and bacteria via proteins like photoactive yellow protein (PYP) (e.g. [7–9]). Such reversible systems can produce more sophisticated sorts of temporal responses than caged compounds.

However, synthetic chromophores that undergo reversible *cis–trans* photoisomerization in isolation have sometimes been found to lose this property when coupled to another molecule [10-15]. For example, Shinkai and colleagues [12–14,16], and Erlanger [17] have studied the behaviour of numerous azobenzene derivatives functionalized with crown ethers and other metal ion-binding groups. The *cis* forms of these compounds bind their targets (metal ions) via electrostatic interactions. In many cases strong target binding inhibits the thermal and photo-chemical *cis*-to-*trans* isomerization process (i.e., the reversibility of the system) [18]. Another example of loss of reversibility was reported by Mascarenas and co-workers who used an azobenzene based cross-linker to artificially dimerize the basic regions of the DNA binding protein GCN4 [11]. The *cis* photoisomer of this construct was found to bind DNA more tightly than the *trans* isomer; however DNA binding was found to completely inhibit the *cis*-to-*trans* photoisomerization and thermal isomerization processes [11]. Very recently, Majima et al have reported introduction using biosynthetic methods of an azobenzene-bearing unnatural amino acid at the dimer interface of the enzyme BamH1 [21]. Regulation of activity was achieved, but again reversibility was compromised.

To be able to design effective, reversibly photo-controlled proteins, we must understand how to avoid this undesirable

* Corresponding author. Tel.: +1 416 978 0675; fax: +1 416 978 0675.
E-mail address: awoolley@chem.utoronto.ca (G.A. Woolley).

1010-6030/$ – see front matter © 2004 Elsevier B.V. All rights reserved.
doi:10.1016/j.jphotochem.2004.12.026

loss of reversibility. Recently, we reported the photo-control of helix content in model peptide systems through the incorporation of a photo-isomerizable azobenzene cross-linking reagent [22-24]. When a thiol-reactive azobenzene cross-linker was combined with a peptide containing Cys residues spaced at positions *i*, *i* + 7 in the primary sequence (designated JRK-X (X—meaning cross-linked)), the dark-adapted cross-linked peptide was predominantly unfolded in water. Upon exposure to light (370 nm) *trans*-to-*cis* isomerization occurred and the peptide became substantially helical as judged by circular dichroism (CD) and nuclear magnetic resonance (NMR) spectroscopy (Fig. 1). When the azobenzene cross-linker was installed between Cys residues spaced at positions *i*, *i* + 11 in the sequence (designated FK-11-X), the opposite behaviour was observed, i.e., *trans*-to-*cis* photoisomerization caused a substantial decrease in helix content [24] (Fig. 1). In contrast to some closely related systems [10,11,21], reversibility of both thermal and photoisomerization were maintained with these peptides. We explore here why this might be so and how such behaviour might be preserved if the cross-linking strategy is applied to other peptide and protein systems.

2. Experimental

2.1. Helix-Coil modelling with AGADIR, FOLDTRAJ and SYBYL

Conformational searches of isolated linkers with methyl groups replacing Cys β atoms were performed using SYBYL (Tripos, Inc.). Systematic searches were performed by rotating all single bonds in the linker in 30° increments. Bond angles and bond lengths were taken from X-ray crystallographic studies [25,26] and high-level computational studies of azobenzene [27]. S–S distances in transition state structures were estimated by setting the N=N bond torsion angle to 90° (rotation) or by setting one N=N–C bond angle to 180° (inversion) [28]. The program AGADIR (http://www.embl-heidelberg.de/Services/serrano/agadir/agadir-start.html) was used to predict overall helicity as well as helix length probabilities. The 'residue fragment' feature of the FOLDTRAJ [29] program was then used to generate an ensemble of peptide structures with helical content distribution matching that predicted by AGADIR [30]. This was accomplished by adding helical fragments of various lengths to the start of the peptide, with probabilities proportional to AGADIR predictions. Effectively this inserts ideal helical segments of varying length into an otherwise randomly generated backbone structure.

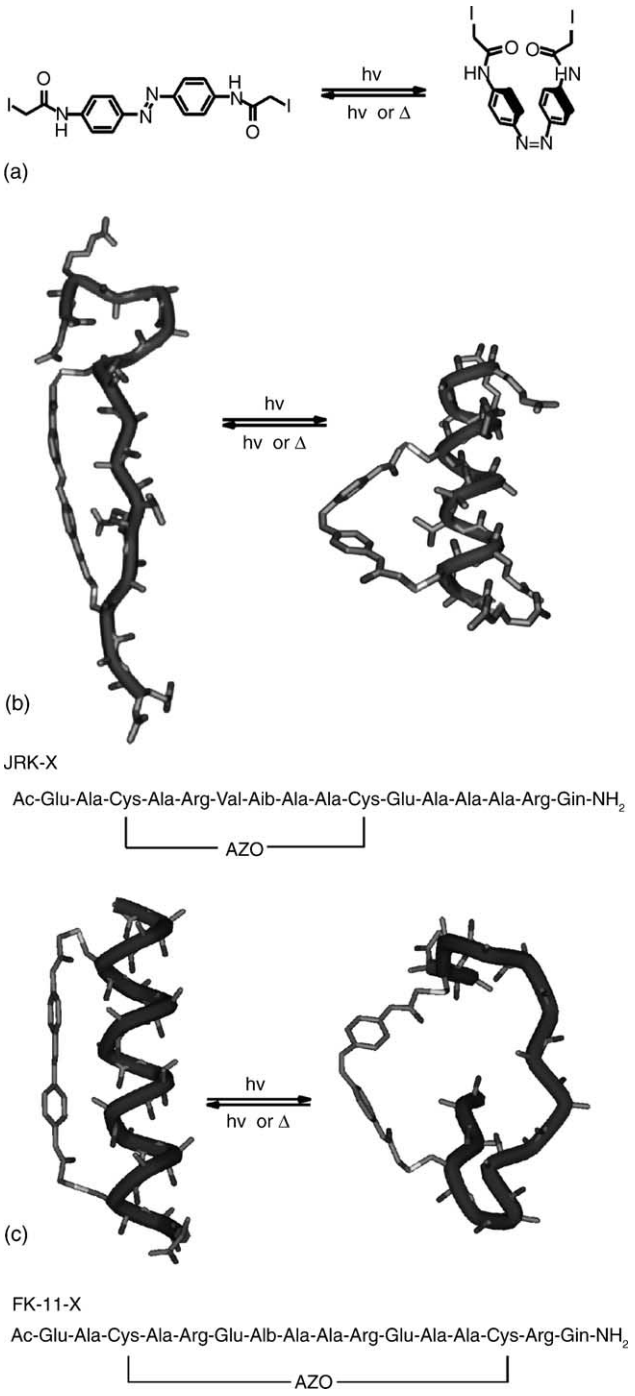

Fig. 1. (a) Chemical structure of the azobenzene containing cross-linker, (b) models showing the increased helicity induced in the JRK-X peptide upon *trans*-to-*cis* isomerization of the attached azobenzene cross-linker. The peptide sequence is shown below the model. (c) Models showing the decreased helicity induced in the FK-11-X peptide upon *trans*-to-*cis* isomerization of the attached azobenzene cross-linker.

2.2. Photokinetic analysis

Solutions (~20 μM) of cross-linked peptide and the control azobenzene-glutathione adduct (prepared as described previously [31]) were prepared in 10 mM sodium phosphate buffer pH 7.0. Absorption spectra were recorded with a diode array UV–vis spectrophotometer (Ocean Optics Inc., USB 2000) coupled to a temperature controlled cuvette holder (Quantum Northwest, Inc.). Irradiation of the sample (at 90° to the light source and detector used for the absorbance

measurements) was carried out using a xenon lamp (450 W) coupled to a double monochromator with slits at 4 nm and 4 nm. Two wavelengths of irradiation (λ_1 = 341 nm and λ_2 = 367 nm), both within the π–π^* absorption band of the chromophore, were chosen for two sets of photokinetic measurements. In the first set, the peptide solution was excited with 341 nm light and the absorbance at 341 and 390 nm was recorded. During the second set, 367 nm light was used for irradiation and the absorbance at 367 nm and 390 nm was monitored. Usually a total irradiation time of 500–600 s was used with a 10 s sampling period. The light intensity in mol/l s at each wavelength of excitation was determined directly in the working cell using an aqueous solution of potassium ferrioxalate [32]. The light used to record the absorbance spectrum was of very low intensity and caused negligible isomerization. The working cell was a quartz cuvette of 1 cm pathlength with a stirring bar at the bottom and contained 1 ml of the peptide solution.

For analysis of the acquired data, a program was written using IDL software (Research Systems Inc.). For numerical integration of the two sets of differential equations the Runge–Kutta (RK4) algorithm was used. Numerical fitting of the experimental data to the photokinetic curves was performed simultaneously using either of two minimization methods – POWELL or AMOEBA [33] (both gave similar results). The rate constants for thermal back isomerization were determined in the dark immediately after the photokinetic experiments at the same temperature.

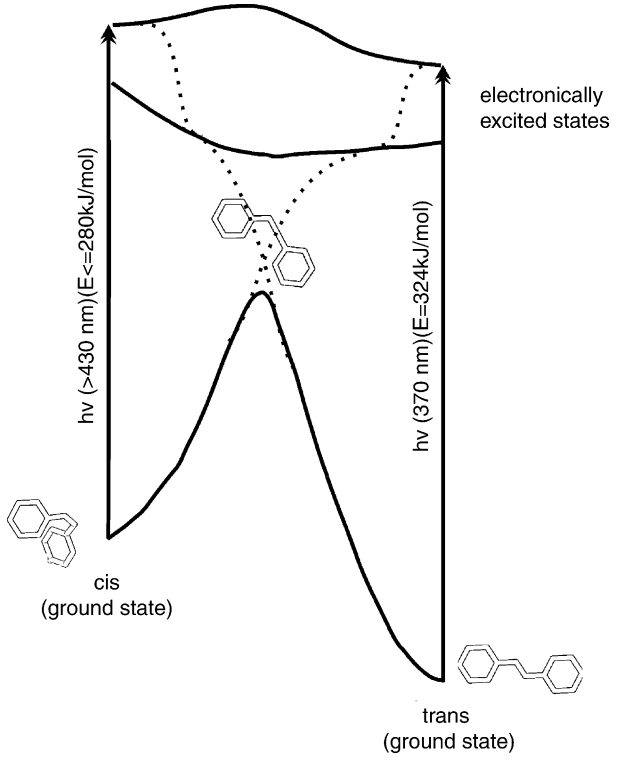

Fig. 2. Simplified energy diagram for the isomerization of azobenzene. The transition state structure shown for the thermal process is that for the inversion mechanism although this has not been unequivocally established ([1,2]).

3. Results

Fig. 2 provides a simplified overview of the isomerization of the azobenzene chromophore [34]. Calorimetric measurements have found the ground state of the unmodified azobenzene chromophore to be more stable in the *trans* conformation by 49 kJ/mol relative to the *cis* state [35]. *Cis*-azobenzene isomerizes to the *trans* form in the dark via a thermal process [36]. Upon irradiation of azobenzene solutions, excited states are produced for which the barriers to *cis*/*trans* isomerization are substantially smaller than the thermal barrier (Fig. 2) [37,38]. Reversion to the electronic ground state (S0) thus produces a mixture of *cis*- and *trans*-azobenzene. If, at the wavelength chosen for irradiation, the trans form absorbs much more strongly than the *cis* form (~360 nm in the present case) then irradiation produces a photostationary state that is substantially *cis* (e.g. 80%). Irradiation at other wavelengths produces photostationary states with different isomer ratios. There is no wavelength for which complete conversion to either isomer can be achieved. No evidence for azobenzene photobleaching was observed during the irradiation times studied in the present case.

Attaching the azobenzene chromophore to another molecule can significantly alter the energy landscape depicted in Fig. 2 as described in the introduction [39]. We consider how attachment to the JRK and FK-11 peptides affects both thermal and photoisomerization in turn.

3.1. Thermal isomerization

We compared the rate of *cis*-to-*trans* isomerization of the cross-linked peptides to the rate of isomerization of the same azobenzene chromophore linked to two glutathione molecules. Glutathione is the common name given to the tri-peptide γGlu–Cys–Gly that occurs as an intracellular mediator of redox potential [40]. It is highly soluble in water but does not adopt any well-defined secondary structure (e.g. helix). The glutathione adduct has the same chemical structure (up to the peptide backbone) as the cross-linked peptides and confers water solubility on the cross-linker so that the isomerization process can be studied under exactly the same solution conditions. Rates of thermal *cis*-to-*trans* isomerization were measured for a series of temperatures by monitoring absorbance at 370 nm after irradiation to convert a percentage of the solution to the *cis* isomer. All curves could be fit well by single exponential decay kinetics. Energies of activation were calculated using the method of Bunce [41] and are collected in Table 1.

To assess how the attached peptides might affect the relative stabilities of the *cis* cross-linker and the transition state, we calculated the distance distribution of the linker attachment points expected for the peptides alone. Fig. 3 shows the

Table 1
Half-lives and activation energies for thermal isomerization

T (°C)	Half-life (min)		
	JRK-X	FK-11-X	G-X (control)
7	112.20	76.70	76.67
15	65.71	41.10	32.85
25	26.74	12.92	11.50
37	7.88	4.26	3.59
45	3.71	1.95	1.74
E_a	77.6 ± 0.6 kJ/mol	74.6 ± 0.5 kJ/mol	74.1 ± 0.5 kJ/mol

distributions of S–S distances in the non-cross-linked JRK and FK-11 peptides expected based on helix-coil theory for peptides with overall helix contents of ∼25% (JRK) and 50% (FK-11). These are the observed helix contents for JRK and FK-11 in non-cross-linked form at low temperatures in water [22]. Also shown for reference are the distance distributions for the same peptides at high temperatures (a limiting "fully denatured" situation). The S–S distance distribution for the JRK peptide with 25% helical content shows a sharp peak at 10.8 Å, the S–S distance for Cys residues spaced i, $i+7$ in a standard α-helix. The S–S distance distribution for the FK-11 peptide with 50% helical content shows a peak near 16.9 Å, the S–S distance for Cys residues spaced i, $i+11$ in a standard α-helix.

We wished to compare these distance distributions with those that can be accommodated by an unperturbed *cis*-cross-linker, a *trans*-cross-linker and a cross-linker with the expected geometry of the inversion and the rotational transition states [1,42]. To estimate what these ranges are, we performed conformational searches by systematically rotating each single bond and determining the ranges of S–S distances in each case. Some representative structures are shown in Fig. 4.

Note that we have not made any attempt to rank the relative energies of these rotameric forms; the intent was simply to examine the range of S–S distances that would be available to the isolated cross-linkers. The energy differences between

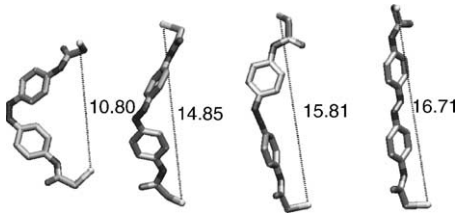

Fig. 4. Representative S–S distances. From left to right: the *cis* cross-linker (left), the rotational transition state, the transition state for inversion and the *trans* cross-linker (right). The bent forms of the cross-linker result in a greater range of S–S distances as single bonds rotate.

single bond rotamers are small compared to the available thermal energy. The S–S distance ranges may be regarded approximate upper bounds although bond angle and bond length vibrations could expand these ranges slightly.

To a first approximation we assume that the cross-linker limits the conformational distribution of the attached peptide to one of these allowed ranges. Thus, a JRK-X peptide with a *cis* cross-linker would have a conformational distribution represented by the section of the full distribution under the bar labelled "*cis*" in Fig. 3a. As discussed previously, this assumption provides a straightforward explanation for the increase in peptide helical content upon *trans*-to-*cis* isomerization of the linker since the spike in the distribution corresponding to highly helical states falls in this region [22,43].

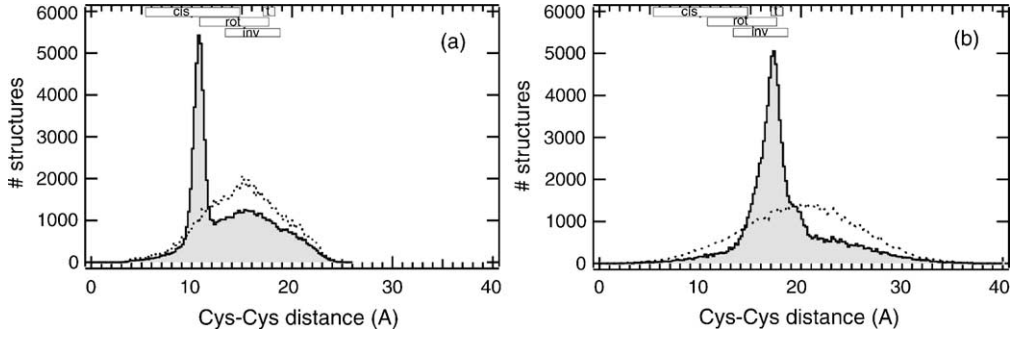

Fig. 3. (a) Histogram showing the distribution of Cys–Cys (S–S) distances (0.2 Å intervals) expected for the non-cross-linked JRK peptide under the conditions of the experiments (overall helix content 25%) (solid line). The dotted line shows the expected distribution for non-cross-linked JRK where the overall helix content is 5% (e.g. at high temperature). (b) Histogram showing the distribution of Cys–Cys (S–S) distances (0.2 Å intervals) expected for the non-cross-linked FK-11 peptide under the conditions of the experiments (overall helix content 50%) (solid line). The dotted line shows the expected distribution for non-cross-linked FK-11 where the overall helix content is 5%. The total number of structures was ∼100,000 in each case. In both (a) and (b), the distance range allowed by a *cis* cross-linker (*cis*); that allowed by a *trans* cross-linker (t), that allowed by a linker in the inversion transition state structure (inv) and that allowed by a rotational transition state (rot) are shown.

Likewise for the FK-11 case the *trans* form of the cross-linker coincides closely with the spike in the distribution at 16.9 Å whereas the *cis*-range does not (Fig. 3b). Thus, *trans*-to-*cis* isomerization causes a decrease in helical content. Our concern here is not with the end states however, but with effects of the peptide conformational distribution on the isomerization process.

A subset of the peptide structures encompassed by the "*cis*-allowed" range (Fig. 3) have S–S distances that are also compatible with the S–S range permitted by a cross-linker with an inversion transition state structure (boxes labelled "inv"). A larger subset of the *cis*-allowed conformations is compatible with S–S range allowed by a cross-linker in a rotational transition state (boxes labelled "rot"). Thermal *cis*-to-*trans* isomerization events of the azo group in the cross-linked peptides would be most likely to occur from one of these subsets of cross-linked peptide conformations. *Cis* peptides outside this range would not isomerize before undergoing fluctuations to achieve an S–S distance compatible with a transition state cross-linker structure. Therefore, to estimate the effect of the attached peptides, JRK and FK-11 on the barriers for thermal isomerization of the cross-linker, we calculated the ratio of the number of conformations in the overlap between the *cis*-range and the inversion transition state range to the number of conformations in the full *cis*-range in each case. We chose to use the inversion subset since this is smaller than the rotation subset and would give an upper limit on the expected size of the effect. For the distributions shown in Fig. 3, this leads to equilibrium constants (#*cis*-range structures/#*cis* ∩ transition state range structures) of $K_{eq} = 5.6$ for JRK-X and $K_{eq} = 2$ for FK-11-X. At 1 °C, this translates into a free energy of stabilization of the *cis* form of the linker relative to the inversion transition state of ∼4 kJ/mol for JRK-X and 1.6 kJ/mol for FK-11-X. The extra stabilization of the *cis* form of the azobenzene cross-linker in JRK-X compared to the glutathione adduct calculated from the experimental data is 4 kJ/mol. For FK-11-X the stabilization is less (0.5 kJ/mol). The experimental data thus matches closely the value calculated from the foregoing simple analysis.

At higher temperatures the peptides have a lower helical content and the S–S distributions become more like those shown by the dashed lines in Fig. 3. Under these conditions, the ratio (#*cis*-range structures/#*cis* ∩ transition state range structures) is somewhat smaller for JRK-X and larger for FK-11-X. Presumably because the effect of temperature on the helix content of the peptide is rather gradual it does not lead to a noticeably nonlinear Arrhenius plot. Instead E_a calculated from the experimental data is probably a low estimate of E_a for *cis*-to-*trans* thermal isomerization of JRK-X at low temperatures and an overestimate for the barrier for isomerization at higher temperatures and vice-versa for FK-11-X.

3.2. Photoisomerization

In order to determine quantum yields for the *trans*-to-*cis* (designated A → B) and the *cis*-to-*trans* (B → A) photoisomerization processes we used the photokinetic method described by Pimienta et al [44]. This approach is particularly useful for the present situation in which there is a thermal process competing with photoisomerization. Three processes were considered to be occurring simultaneously when a solution of cross-linked peptide or the glutathione control was continuously irradiated and stirred:

Photoisomerization:

$$\mathrm{A} \rightarrow \mathrm{B}; \quad \text{with a rate} \quad v_1 = \phi_{AB}\varepsilon_A(\lambda_{ex})[A]lFI_0 \tag{1}$$

Photo-induced back isomerization:

$$\mathrm{B} \rightarrow \mathrm{A}; \quad \text{with a rate} \quad v_2 = \phi_{BA}\varepsilon_B(\lambda_{ex})[B]lFI_0 \tag{2}$$

Thermal back isomerization:

$$\mathrm{B} \rightarrow \mathrm{A}; \quad \text{with a rate} \quad v_3 = k_{BA}[B] \tag{3}$$

where ϕ_{AB} and ϕ_{BA} are quantum yields, $\varepsilon_A(\lambda_{ex})$ and $\varepsilon_B(\lambda_{ex})$ are the extinction coefficients at the excitation wavelength, [*A*] and [*B*] are concentrations, *l* is the optical pathlength of the sample (1 cm), I_0 is the intensity of the excitation, k_{BA} is the rate constant for thermal back isomerization (determined above) and *F* is the photokinetic factor:

$$F = \frac{1 - 10^{-\mathrm{OD}(\lambda_{ex})}}{\mathrm{OD}(\lambda_{ex})} \tag{4}$$

where (OD(λ_{ex})) is the optical density at the excitation wavelength. The kinetic equation for the rate of change of [*A*] is given by:

$$\frac{\mathrm{d}[A]}{\mathrm{d}t} = -v_1 + v_2 + v_3 \tag{5}$$

Using this rate equation together with the Beer–Lambert law for absorbance of the photoreaction mixture at any wavelength:

$$\mathrm{OD}(\lambda) = \varepsilon_A(\lambda)[A]l + \varepsilon_B(\lambda)[B]l, \tag{6}$$

and the equation for the conservation of matter at any moment of irradiation:

$$[A] + [B] = [A]_0, \tag{7}$$

the parameters ϕ_{AB}, ϕ_{BA} and $\varepsilon_B(\lambda_{ex})$ as well as the absorbance spectrum of B can be extracted from a numerical analysis of the photokinetic curves (plots of absorbance versus time under continuous irradiation). Two sets of photokinetic curves corresponding to two different wavelengths of irradiation must be determined. These two wavelengths must lie in the same absorption bands for both A and B. In addition, the dark adapted spectrum of A as well as the spectrum of the reaction mixture at the last acquisition time during irradiation must be recorded so that the spectrum of B may be calculated.

With realistic starting values of the unknown parameters, the differential Eq. (5) was integrated numerically for each set of measurements. Then the solutions were applied to Eqs. (6) and (7) to obtain simulated curves of OD versus *t*. Then,

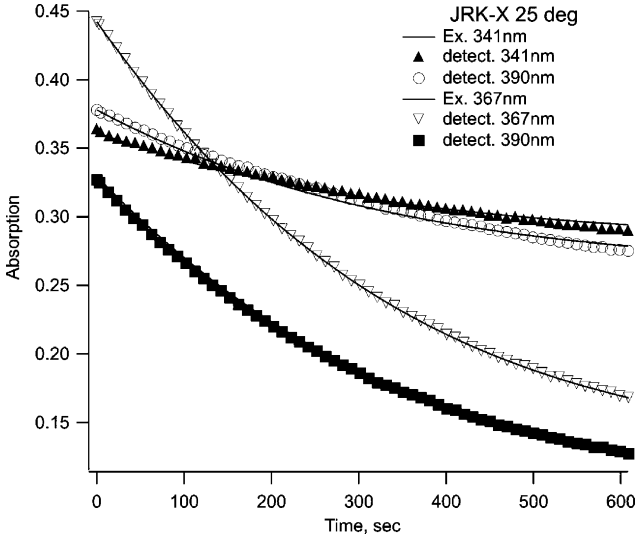

Fig. 5. A set of photokinetic curves obtained for JRK-X at 25 °C (10 mM phosphate buffer, pH 7.0). Experimental points are plotted as symbols; calculated fits are lines.

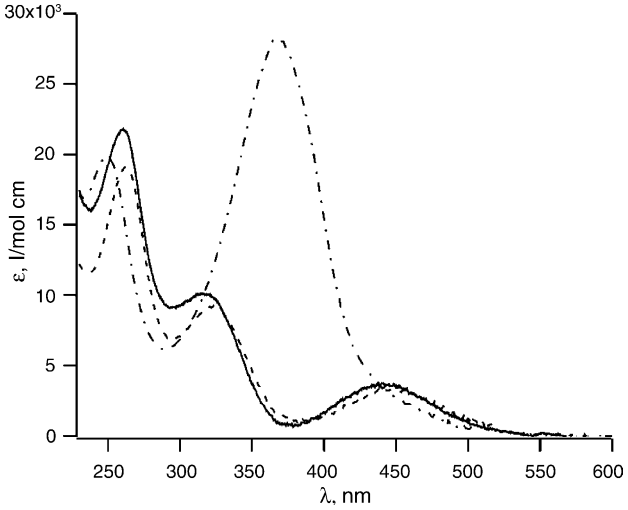

Fig. 6. Calculated (solid line) and experimental (dashed line) adsorption spectrum of the *cis* isomer of JRK-X. The spectrum of the *trans* form (dash–dot line) is shown for reference. Similar spectra were obtained for FK-11-X.

the parameters ϕ_{AB}, ϕ_{BA} and $\varepsilon_B(\lambda_{ex})$ were optimized in an iterative procedure designed to minimize the residual error (calculated as the sum of squares of differences between the simulated and experimental curves). A representative set of curves obtained for the cross-linked JRK-X peptide irradiated in the π–π^* band is shown in Fig. 5.

The quantum yields derived from this fitting procedure are collected in Table 2. Note that increases in ϕ_{BA} (*cis* → *trans*) are seen for both JRK-X and FK-11-X compared to the azobenzene linker attached to glutathione (G-X). A smaller absolute effect, but in the opposite direction is observed for ϕ_{AB}(*trans* → *cis*).

To calculate the absorption spectrum of the unstable isomer B (*cis*) one needs to know the value of ε_B at any λ which is obtained after the curve fitting process. Then, the concentrations of A and B in the photoreaction mixture can be calculated from Eqs. (6) and (7) at any time during the irradiation. The desired spectrum is then the absorption spectrum of the reaction mixture at any time minus the spectrum of A (the pure *trans* isomer) multiplied by its fraction at the same moment of time. This procedure for calculating the spectrum of B (*cis* isomer) serves as an independent check of the entire fitting procedure since a spectrum of the pure *cis* isomer can be directly obtained by rapid separation of *cis* and *trans* states using a diode-array spectrophotometer coupled to a high performance liquid chromatograph. Fig. 6 shows that the calculated and experimental spectra of the pure *cis* isomers agree closely except for below 300 nm where differences in the solvent and buffer conditions between the HPLC and the photokinetic experiments cause intensity shifts although spectral shape is preserved.

4. Discussion

One source of the difference in the apparent reversibility of the present system compared to some of those examined previously may be the chemical nature of the chromophore used in each case. Although both systems employed azobenzene derivatives, the amide-substituted azobenzene derivatives studied here have intrinsically smaller thermal barriers for isomerization than alkyl substituted, ether substituted or carbonyl substituted derivatives [14,45]. Photoisomerization quantum yields, however are similar for this chromophore and other azobenzenes [46,47].

In considering the thermal isomerization process, a central question is how the attached molecule affects the relative stabilities of the *cis* ground state and the transition state for the *cis*-to-*trans* thermal process. With the compounds studied by Shinkai, the *cis* forms bind their targets (metal ions) via

Table 2
Quantum yields for photoisomerization (π–π^* irradiation)

T (°C)	JRK-X		FK-11-X		G-X (control)	
	ϕ_{AB} (*trans* → *cis*)	ϕ_{BA} (*cis* → *trans*)	ϕ_{AB} (*trans* → *cis*)	ϕ_{BA} (*cis* → *trans*)	ϕ_{AB} (*trans*→*cis*)	ϕ_{BA} (*cis*→*trans*)
1	0.07 ± 0.01	0.47 ± 0.05	0.07 ± 0.01	0.50 ± 0.05	0.10 ± 0.01	0.39 ± 0.03
25	0.10 ± 0.01	0.49 ± 0.05	0.08 ± 0.01	0.62 ± 0.06	0.12 ± 0.01	0.38 ± 0.03
37	0.11 ± 0.01	0.54 ± 0.06	0.09 ± 0.01	0.63 ± 0.07	0.14 ± 0.01	0.43 ± 0.04

electrostatic interactions. It is clear that if these stabilizing interactions are removed in the transition state a higher barrier to thermal reversion will inevitably result [18].

Thus, thermal reversibility appears to be preserved in this case because easily accessible peptide conformations exist in which the normal transition state for inversion (or rotation) can be accommodated. Single bonds provide flexibility in the azo linker structure so that the transition state is compatible with a significant range of peptide S–S distances. However, as intrinsic peptide helical content increases, the S–S distance range will tend to encompass less of the distance range required for access to a transition state (particularly an inversion transition state) so that thermal *cis*-to-*trans* isomerization would be more and more inhibited. Of course, as the temperature is increased, the helix content of even highly helical peptides is likely to decrease permitting access to S–S distances that would permit inversion of the azo linker. A corollary of the foregoing is that attachment of the azobenzene cross-linker to a peptide or protein may alter the relative stabilities of transitions states for inversion and for rotation and so may in fact influence the isomerization mechanism. As the constraints of the *cis* form of the chromophore become more stringent in terms of S–S distance, a rotational pathway may be favoured owing to the greater overlap in compatible S–S distances.

4.1. Photoisomerization

The photoisomerization process is essentially different from the thermal process in that ~330 kJ/mol of energy is deposited upon absorption of 365 nm photons. In the present case only π–π^* excitation was studied since π–π^* excitation would be employed during application of these molecules as biochemical photo-switches. In contrast to the thermal case, the peptide conformational ensemble is unlikely to be relaxed with respect to the transition state structures of the azobenzene group. Time resolved optical rotatory dispersion measurements and infrared measurements on these systems [48,49] have shown clearly that peptide conformational changes occur more than four orders of magnitude more slowly than the linker isomerization event. The effect of the peptide on the photochemical *cis*-to-*trans* isomerization process must therefore reflect effects of the *cis* (ground state) peptide conformational distribution on the excited state energy landscape. Likewise, any effects of the peptide on the photochemical *trans*-to-*cis* isomerization process must reflect effects of the *trans* (ground state) peptide conformational distribution on the excited state energy landscape.

As noted above, attachment of azobenzene groups to ion chelators and DNA-binding peptides has caused inhibition of photoisomerization, presumably because the structure inhibits motion along any coordinate (rotation or inversion) in the excited state. In the present case, *trans*-to-*cis* photoisomerization is slightly inhibited by attachment to both the JRK peptide and the FK-11 peptide but an increased quantum yield for *cis*-to-*trans* isomerization is observed for both peptides compared to the glutathione adduct. A detailed analysis of the origins of these effects is complicated by that fact that even for unmodified azobenzene, the relative energies of different excited states and the barriers to their interconversion continue to be subjects of lively discussion [2,28,34,50–52]. A few studies have examined how the structure of an attached molecule can alter the quantum yield for azobenzene photoisomerization [1,39,42]. Specifically, increased quantum yields for *trans*-to-*cis* photoisomerization have been observed previously with azo compounds in which a rotational transition state was expected to be sterically inhibited and an inversion transition state allowed [1,42]. However, it is not clear that the azobenzene derivatives employed by these authors do in fact sterically prevent rotation since analogous stilbene derivatives (where inversion cannot occur) still isomerize [53,54]. Instead, reduced rotational freedom of azobenzene phenyl rings in these derivatives has been proposed to lead to increased quantum yields [34,42].

The observation of an increased quantum yield for *cis*-to-*trans* isomerization implies either that the *cis* peptide conformation enhances productive *cis*-to-*trans* photoisomerization or inhibits a pathway to S0. Various characteristic motions of helical peptides including longitudinal vibrations of α-helices occur on the picosecond timeframe [55,56]. These motions may couple productively with an isomerization coordinate to increase the quantum yield. As the temperature is increased, however, the helix content decreases substantially [22] whereas the observed quantum yield increases (Table 2). Thus, perhaps, as described above, the attached peptide instead inhibits a dynamic mode of the azobenzene chromophore and thereby inhibits deactivation to S0.

In any case, the observed effects of the attached peptides on quantum yields for photoisomerization in either direction are not very large and in no case is isomerization substantially inhibited. This feature of the systems – vital from the standpoint of the design of an effective biological photoswitch – can be understood to a first approximation in the same manner as described above for the thermal isomerization process. The flexibility of the peptide attachment is such that relatively unperturbed transition states can be accessed through rotation of a few single bonds. Both the photoisomerization process and the thermal isomerization process are therefore not much changed from that undergone by the unattached chromophore. As can be seen from the analysis presented in the Results section the effects of these model peptides on the barriers to *cis*-to-*trans* thermal isomerization can be predicted semi-quantitatively simply by considering how the S–S distances in the intrinsic conformational distributions of the peptides overlap with S–S distance ranges of the chromophore in its various forms. The same approach could be applied to other designed photoswitches if a reliable estimate of the conformational dynamics of the target could be obtained either through experiment (e.g. NMR analysis) or molecular simulation. In this way, one may be able to avoid the creation of photoswitches where reversibly is compromised.

Acknowledgements

We would like to thank the Natural Sciences and Engineering Research Council of Canada (GAW). Modelling support was provided by the Molecular Design and Information Technology (MDIT) Centre (Toronto).

References

[1] H. Rau, E. Luddecke, J. Am. Chem. Soc. 104 (1982) 1616–1620.
[2] A. Cembran, F. Bernardi, M. Garavelli, L. Gagliardi, G. Orlandi, J. Am. Chem. Soc. 126 (2004) 3234–3243.
[3] S.R. Adams, R.Y. Tsien, Annu. Rev. Physiol. 55 (1993) 755–784.
[4] K. Curley, D.S. Lawrence, Pharmacol. Ther. 82 (1999) 347–354.
[5] Y. Shigeri, Y. Tatsu, N. Yumoto, Pharmacol. Ther. 91 (2001) 85–92.
[6] E.M. Callaway, R. Yuste, Curr. Opin. Neurobiol. 12 (2002) 587–592.
[7] K.J. Hellingwerf, W.D. Hoff, W. Crielaard, Mol. Microbiol. 21 (1996) 683–693.
[8] U.K. Genick, S.M. Soltis, P. Kuhn, I.L. Canestrelli, E.D. Getzoff, Nature 392 (1998) 206–209.
[9] E. Schafer, C. Bowle, EMBO Rep. 3 (2002) 1042–1048.
[10] R. Cerpa, F.E. Cohen, I.D. Kuntz, Fold. Des. 1 (1996) 91–101.
[11] A.M. Caamano, M.E. Vazquez, J. Martinez-Costas, L. Castedo, J.L. Mascarenas, Angew. Chem. Int. Ed. Engl. 39 (2000) 3104–3107.
[12] S. Shinkai, S. Nakamura, M. Nakashima, O. Manabe, M. Iwamoto, Bull. Chem. Soc. Jpn. 58 (1985) 2340–2347.
[13] S. Shinkai, T. Ogawa, Y. Kusano, O. Manabe, K. Kikukawa, T. Goto, T. Matsuda, J. Am. Chem. Soc. 104 (1982) 1960–1967.
[14] S. Shinkai, T. Minami, Y. Kusano, O. Manabe, J. Am. Chem. Soc. 105 (1983) 1851–1856.
[15] O. Ohtania, T. Furukawaa, R. Sasaib, E. Hayashic, T. Shichia, T. Yuia, K. Takagi, J. Mater. Chem. 14 (2004) 196–200.
[16] S. Shinkai, in: H. Dugas (Ed.), Bioorganic Chemistry Frontiers, 1, Springer–Verlag, Berlin, 1990, pp. 161–195.
[17] M. Blank, L.M. Soo, H.N. Wassermann, B.F. Erlanger, Science 214 (1981) 70–72.
[18] S. Shinkai, O. Manabe, in: F. Vogtle, E. Weber (Eds.), Host Guest Complex Chemistry III, Springer–Verlag, Berlin, 1984, pp. 67–104.
[21] K. Nakayama, M. Endo, T. Majima, Chem. Commun. (Camb.) (2004) 2386–2387.
[22] J.R. Kumita, O.S. Smart, G.A. Woolley, Proc. Natl. Acad. Sci. USA 97 (2000) 3803–3808.
[23] J.R. Kumita, D.G. Flint, O.S. Smart, G.A. Woolley, Protein Eng. 15 (2002) 561–569.
[24] D.G. Flint, J.R. Kumita, O.S. Smart, G.A. Woolley, Chem. Biol. 9 (2002) 391–397.
[25] J.M. Robertson, J. Chem. Soc. (1939) 232–236.
[26] C.J. Brown, Acta Cryst. 21 (1966) 146–152.
[27] H. Fliegl, A. Kohn, C. Hattig, R. Ahlrichs, J. Am. Chem. Soc. 125 (2003) 9821–9827.
[28] T. Ikegami, N. Kurita, H. Sekino, Y. Ishikawa, J. Phys. Chem. A 107 (2003) 4555–4562.
[29] H.J. Feldman, C.W. Hogue, Proteins 46 (2002) 8–23.
[30] V. Munoz, L. Serrano, Biopolymers 41 (1997) 495–509.
[31] Z. Zhang, D.C. Burns, J.R. Kumita, O.S. Smart, G.A. Woolley, Bioconjug. Chem. 14 (2003) 824–829.
[32] C.G. Hatchard, C.A. Parker, Proc. R. Soc. London, Ser. A 235 (1956) 518–536.
[33] W.H. Press, S.A. Teukolsky, W.T. Vetterling, B.P. Flannery, Numerical Recipes in C, 2nd ed., Cambridge University Press, Cambridge, 1992.
[34] T. Schultz, J. Quenneville, B. Levine, A. Toniolo, T.J. Martinez, S. Lochbrunner, M. Schmitt, J.P. Shaffer, M.Z. Zgierski, A. Stolow, J. Am. Chem. Soc. 125 (2003) 8098–8099.
[35] A.R. Dias, M.E. Minas da Piedade, J.A. Martinho Simoes, J.A. Simoni, C. Teixeira, H.P. Diogo, Y. Meng-Yan, G. Pilcher, J. Chem. Thermodyn. 24 (1992) 439–447.
[36] H. Rau, in: H. Durr, H. Bouas-Laurent (Eds.), Photochromism. Molecules and Systems, Elsevier, Amsterdam, 1990, pp. 165–192.
[37] H. Rau, in: J.F. Rabek (Ed.), Photochemistry and Photophysics, Vol. II, CRC Press Inc, Boca Raton, FL, 1990, pp. 119–141.
[38] S. Sporlein, H. Carstens, H. Satzger, C. Renner, R. Behrendt, L. Moroder, P. Tavan, W. Zinth, J. Wachtveitl, Proc. Natl. Acad. Sci. USA 99 (2002) 7998–8002.
[39] J. Wachtveitl, S. Sporlein, H. Satzger, B. Fonrobert, C. Renner, R. Behrendt, D. Oesterhelt, L. Moroder, W. Zinth, Biophys. J. 86 (2004) 2350–2362.
[40] A. Meister, M.E. Anderson, Annu. Rev. Biochem. 52 (1983) 711–760.
[41] N.J. Bunce, C.L. Forber, C. McInnes, J.M. Hutson, J. Chem. Soc., Perkin Trans. II 3 (1988) 363–368.
[42] I.K. Lednev, T.Q. Ye, L.C. Abbott, R.E. Hester, J.N. Moore, J. Phys. Chem. 102 (1998) 9161–9166.
[43] D.C. Burns, D.G. Flint, J.R. Kumita, H.J. Feldman, L. Serrano, Z. Zhang, O.S. Smart, G.A. Woolley, Biochemistry 43 (2004) 15329–15338.
[44] V. Pimienta, D. Lavabre, G. Levy, A. Samat, R. Guglielmetti, J.C. Micheau, J. Phys. Chem. 100 (1996) 4485–4490.
[45] N. Nishimura, T. Sueyoshi, H. Yamanaka, E. Imai, S. Yamamoto, S. Hasegawa, Bull. Chem. Soc. Jpn. 49 (1976) 1381–1387.
[46] G. Zimmerman, L. Chow, U. Paik, J. Am. Chem. Soc. 80 (1958) 3528–3531.
[47] S. Yamashita, H. Ono, O. Toyama, Bull. Chem. Soc. Jpn. 35 (1962) 1849–1853.
[48] E. Chen, J.R. Kumita, G.A. Woolley, D.S. Kliger, J. Am. Chem. Soc. 125 (2003) 12443–12449.
[49] J. Bredenbeck, J. Helbing, J.R. Kumita, G.A. Woolley, P. Hamm, Proc. Natl. Acad. Sci. USA (2005), in press.
[50] N. Tamai, H. Miyasaka, Chem. Rev. 100 (2000) 1875–1890.
[51] C. Ciminelli, G. Granucci, M. Persico, Chemistry 10 (2004) 2327–2341.
[52] C.W. Chang, Y.C. Lu, T.T. Wang, E.W. Diau, J. Am. Chem. Soc. 126 (2004) 10109–10118.
[53] Y. Norikane, K. Kitamoto, N. Tamaoki, J. Org. Chem. 68 (2003) 8291–8304.
[54] D. Tanner, O. Wennerstrom, Tet. Lett. 22 (1981) 2313–2316.
[55] R.M. Levy, M. Karplus, Biopolymers 18 (1979) 2465–2495.
[56] J.A. Fornes, S.R. Massanes, Phys. Chem. Chem. Phys. 5 (2003) 624–631.